Ionization and dissociation of N_2 and CO in collisions with 2.3q-keV Ar^{q+} ($8 \leq q \leq 14$)

J. Vancura and V. O. Kostroun
Nuclear Science and Engineering Program, Ward Laboratory, Cornell University, Ithaca, New York 14853
(Received 16 August 1993)

The charge-state and energy distribution of molecular ions and fragments produced in low-energy, highly-charged-argon-ion collisions with N_2 and CO were measured. Ar^{q+} ($8 \leq q \leq 14$) ions produced by an electron-beam ion source and extracted at 2.3 kV interacted with a molecular-target gas jet located in the ionization region of a time-of-flight spectrometer. The resulting molecular recoils and fragments were analyzed by time of flight. For a given molecular target, the measured spectra are all similar and do not depend on the incident argon-projectile charge state. The spectra are dominated by the singly charged ion, either N_2^+ or CO^+. The stable or long-lived metastable doubly charged molecular ion CO^{2+} is the second most prominent feature in Ar^{q+} on the CO spectra. Similarly, N_2^{2+}, which cannot be distinguished from N^+, is also presumed to be present in Ar^{q+} on the N_2 spectra. The remaining peaks are associated with the dissociation of the N_2^{Q+} and CO^{Q+} ($2 \leq Q \leq 6$) molecular ions formed in the collision. The peak positions correspond to fragments of a given mass-to-charge ratio and kinetic energy calculated assuming vertical target ionization.

PACS number(s): 34.50.−s, 35.80.+s, 34.90.+q, 82.30.Fi

I. INTRODUCTION

Collisions of highly charged ions with few- and multielectron atomic targets have been investigated by numerous groups over the past two decades. Following such collisions, the projectiles typically retain their charge or gain one or two electrons, while the target atoms have been observed in much higher states of ionization. The details of the outcome of the collision as well as the pertinent fundamental processes involved depend on the relative velocity between the target and the projectile. Both theoretical and experimental aspects of such collisions have been discussed in recent review articles [1–3].

On the other hand, collisions of highly charged ions with simple homo- or heteronuclear diatomic molecules (O_2,N_2,CO,NO) have attracted less attention. Wohrer *et al.* [4] studied fragmentation of CO^{Q+} molecular ions produced in collision with 97 MeV Ar^{14+} by the ion-ion coincidence time-of-flight (TOF) technique. Their results show that for $Q \geq 2$, breakup of the molecular ions preferentially leads to a symmetric or nearly symmetric distribution of charge between the fragments. The TOF spectra are dominated by dissociation products, with C^+ and C^{2+} peaks being the most prominent. The molecular ions CO^+ and especially CO^{2+} do not seem to be formed in any appreciable quantities. In an earlier paper, this group investigated the Coulomb explosion of O_2^{Q+} molecular ions following 40 MeV Ar^{13+} collisions with O_2 [5]. Ben-Itzhak, Ginther, and Carnes [6] have also investigated the CO^{Q+} system produced in collisions of 1 MeV/amu F^{4+} ions with CO, using the ion-coincidence TOF technique. The TOF spectra show the molecular-ion CO^+ as being dominant, followed by the dissociation products C^+, O^+, C^{2+}, O^{2+}, etc, whose intensities are smaller by at least an order of magnitude. The CO^{2+} peak, which is comparable in intensity to the C^{2+} fragment peak, seems to be more pronounced than in the experiment of Wohrer *et al.* [4]. The most probable reason for this enhancement is the lower energy per amu of the incident fast ion beam [6]. In Refs. [4] and [6], the relative cross sections for the single dissociation channels were measured. Using a quadrupole mass spectrometer. Mathur *et al.* [7] recorded recoil-ion spectra and measured the energy distributions of recoil ions produced in 100 MeV collisions of Si^{8+} with CO_2 and CS_2 molecules. Varghese *et al.* [8] studied collisions of 19 MeV F^{9+} ions with N_2. Using two-dimensional detection of the recoil ions and their fragments, these authors investigated the alignment of the molecular axis with respect to the incident projectile direction prior to the Coulomb explosion.

The molecular recoil-ion charge-state spectroscopy measurements involving highly charged ions have been, thus far, confined to fast collisions in the MeV range. If one disregards experiments on state-selective electron capture in low-energy, highly charged ion-molecular hydrogen (deuterium) collision [1,2], experiments on heavier molecular targets are almost nonexistent. Soejima *et al.* [9] have measured cross sections for single and multiple electron capture by the projectile in collisions of C^{4+} with H_2, N_2, and O_2 in the 0.33–666 eV/amu collision energy range. McLaughlin, McCullough and Gilbody [10] have studied collisions of C^{4+} with H_2 and O_2 at 4–6 keV by medium-resolution, 4-eV, translational spectroscopy. In their interpretation of the energy gain spectra, the authors concentrated on the dominant single electron-capture channels. Transfer ionization processes which lead to highly ionized or dissociated recoil ions appear to be of minor importance and only show up as peak tails that extend toward higher exoergicity values. As far as higher projectile charge states are concerned, the preliminary results of Ar^{11+} on N_2 and CO collisions at 2.3q keV by Vancura and Kostroun [11], and the recent work on Ar^{8+} on CO_2 at 2.0q keV by Lebius and Huber [12] appear to be the only such experiments reported to date.

Collision of multiply charged ions with atomic and molecular hydrogen, helium, and the lighter noble gases at relative velocities much smaller than 1 a.u. are dominated by electron transfer from the target to the projectile. For example, collisions of $2.3q$ keV Ar^{q+} ($8 \leq q \leq 16$) with argon indicate that up to eight electrons can be removed from the target in a single collision [13]. Furthermore, the electron-capture cross sections are large, on the order of 10^{-14} cm^2. The process of single-electron capture by bare, hydrogen and heliumlike ions of low to medium Z elements with atomic and molecular hydrogen and helium is thought to be well understood [1,2], and is essentially an extension of existing theories of electron capture by singly charged ions. Capture is described in terms of electron transitions between molecular orbitals of the quasimolecule formed during the collision. Diabatic transitions at pseudocrossings of the ingoing potential-energy curve with the large number of outgoing potential-energy curves provide the mechanism responsible for charge transfer. As far as two or more electron capture is concerned, no satisfactory theoretical descriptions of such processes exist at present.

In order to better understand the mechanism of multielectron transfer from many electron targets, it is of interest to investigate collisions of highly-charged-argon ions with multielectron atomic and molecular targets. If one considers the duration of the interaction of a multicharged ion with a molecule, then the several hundred eV per charge or lower projectile energy region is of interest. Furthermore, collisions of low-energy, highly charged ions with simple but heavier molecular targets could be used to gain a better understanding of the mechanisms of electron transfer in collisions with multielectron atomic targets or vice versa. Thus, it is of interest to compare the difference in behavior of atomic and molecular targets in greater detail. Finally, the doubly charged molecular ions O_2^{2+}, N_2^{2+}, CO^{2+}, and NO^{2+}, which are some of the more interesting collision products produced, have been studied extensively both experimentally and theoretically over the past years and are themselves of intrinsic interest [14,15].

In his paper, we report on measurements of the charge state and energy distribution of molecular ions and fragments in low-energy, highly-charged-argon-ion molecular collisions with N_2 and CO. Ar^{q+} ($8 \leq q \leq 14$) ions produced by an electron-beam ion source (EBIS) interacted with a target gas effusing from a jet in the ionizing region of a time-of-flight spectrometer. The resulting molecular recoils and their fragments were analyzed by time of flight.

II. EXPERIMENTAL METHOD

A. Experimental arrangement

Low-energy, highly charged Ar^{q+} ($8 \leq q \leq 14$) ions were produced by the Cornell superconducting-solenoid, cryogenic electron-beam ion source CEBIS [16] and extracted at 2.3 kV. In an electron-beam ion source, ions are formed by sequential ionization by electron impact. Ions are trapped radially by the space-charge potential of a high current-density electron beam focused by a solenoidal magnetic field. They are trapped axially by a potential distribution applied to a drift tube structure which consists of cylindrical electrodes concentric with the electron beam. After a preset confinement time (20 to 100 ms), the axial trap potential distribution is modified, and the ions are extracted from the source. The extracted ion pulse is typically 50 μsec long. In our experiments, we used a 17-mA, 3.8-keV electron beam (-1.5 kV on the electron gun cathode, and $+2.3$ kV on the cylindrical electrode drift tube structure). The extracted ion pulse repetition frequency ranged from 9 to 47 Hz.

The extracted ions were charge selected by a 90° bending magnet. At the downstream magnet focus is a pair of adjustable chopper plates (Fig. 1). One of the plates was biased at 10 V negative, with respect to ground, to deflect the ion beam so that it would not pass through a 0.8-mm-wide, 5-mm-high TOF spectrometer entrance slit located 40 cm downstream from the plates. To select a narrow time slice from the tens of microseconds long ion pulse extracted from the EBIS, a 200–800-ns-long, rectangular, positive 10-V pulse was applied to the plate biased at 10 V negative. The pulse brought the potential between the chopper plates to zero, and ions could pass through the TOF spectrometer entrance slit. The chopper plate pulse was triggered by the signal which initiated the EBIS ion extraction cycle.

The few-hundred-ns-long pulse of projectile ions then entered the ionization or interaction region of the TOF spectrometer. The beam of ions interacted with a target gas, injected at right angles to the beam through an effusive jet with a rectangular nozzle 0.5 mm wide, and 10 mm long. The effusive jet was located 21 mm downstream from the spectrometer entrance slit. Molecular ions and their charged fragments, produced in collisions

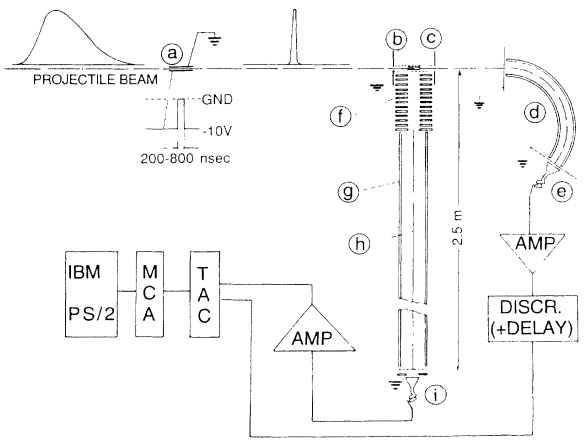

FIG. 1. Experimental arrangement used to measure the charge-state and energy distribution of molecular ions and fragments produced in low-energy collisions of highly charged argons ion with N_2 and CO. (a) Chopper plates, (b) repeller, (c) effusive gas jet, (d) $\pi/\sqrt{2}$ cylindrical electrostatic analyzer, (e) channeltron, (f) accelerator column, (g) time-of-flight tube, (h) guide wire, (i) channeltron. The signals were amplified (AMP) and fed into a time-to-amplitude converter. Output pulses from the TAC were processed by a multichannel analyzer.

of highly charged projectiles with the target gas were then extracted from the interaction region by an electric field of a few V/cm and analyzed by TOF. The TOF spectrometer is biased on the Wiley-McLaren design [17]. The extraction field is applied between two circular electrodes, 51 mm o.d. and 28.6 mm i.d., separated by 14.6 mm. The interaction region is defined by the intersection of the projectile beam and gas jet located midway between these two electrodes. Both electrode apertures are covered by 90% transmission stainless-steel mesh. The mesh guarantees field uniformity in the interaction region, as well as almost 100% spectrometer acceptance of thermal energy ions. Upon entering the spectrometer, the recoil ions were accelerated by a 84.5-mm-long acceleration column which consists of 12 ring shaped electrodes similar to those used to define the interaction region. The last electrode is covered with 90% transmission stainless-steel mesh and is biased at the same potential as the TOF tube. The 2350-mm-long TOF tube has a central guide wire which is biased at several volts negative with respect to the tube. The guide wire traps the ions radially, but does not change their flight time [18]. The ions and charged fragments were detected by a channeltron multiplier operated in the pulse-counting mode. The TOF spectrometer, which is electrically isolated from ground, is housed in a 10-cm-o.d. stainless-steel tube.

After passing through the TOF spectrometer interaction region, the incident beam was analyzed by a $\pi/\sqrt{2}$ cylindrical electrostatic analyzer located 35 cm downstream from the interaction region. The $\pi/\sqrt{2}$ cylindrical electrostatic analyzer was mounted on a movable stage, and could be displaced to compensate for the deflection of the beam caused by the extracting field in the interaction region.

The apparatus was pumped on by two 170-l/s (air) Balzers turbomolecular pumps and a 1000-l/s (air) Varian VK12A cryopump. One turbomolecular pump was located in the middle of the long TOF tube. The other pump, along with the cryopump, pumped on the main vacuum chamber, a 15-cm-i.d., six-way stainless-steel cross. The gas target jet nozzle was located directly above the cryopump. With the gas jet turned off, the base pressure in the vacuum chamber was in the low-10^{-9}-mbar range. With the jet on, the background pressure in the main vacuum chamber and the TOF tube rose to the low-10^{-7}-mbar range. Assuming a total-cross-section σ of 5×10^{-15} cm^2 for very low energy, highly charged ions interacting with the background gas, a 2.5-m-long flight path l and a target density n of 2.5×10^{9} per cm^3 at 10^{-7} mbar, $\sigma ln=0.031$, which satisfies the single-collision condition.

B. Data acquisition and time-of-flight spectrometer calibration

The signal from the channeltron on the $\pi/\sqrt{2}$ cylindrical electrostatic analyzer set to analyze the projectile beam provided the start pulse, and the TOF channeltron the stop pulse for an ORTEC 457 time-to-amplitude converter. The channeltron start signals were amplified by an ORTEC 485 amplifier, and then fed into an ORTEC 551 timing single-channel analyzer. The stop signals from the TOF channeltron were amplified by an ORTEC VT120A fast preamplifier and used without further processing. The output pulses from the time-to-amplitude converter were analyzed by an ORTEC 916-A multichannel analyzer plug-in card for an IBM PS/2 Model 30 computer and MAESTRO II MCA emulation software.

To obtain the best signal-to-noise ratio TOF spectra, the incident ion beam had to be deflected completely off the spectrometer entrance slit. This was done by manually adjusting the separation between the chopper plates, as well as the beam position with respect to the plates. (The signal-to-noise ratio could have been improved by amplifying the 4-ns rise-time pulse applied to the chopper plate, but mechanical adjustment of the plates was simpler.)

The resolution of the TOF spectrometer used in the experiment depends on the ratio of the width of the chopper pulse to the total flight time, and on the potential applied to the guide wire. The effect of the guide wire on the time of flight and transmission through the spectrometer was investigated by numerical calculation of ion trajectories [19]. The calculations clearly showed the spiral trajectories with different path lengths for individual ions propagating down the drift tube. The different path lengths give different flight times, thereby broadening the TOF peaks. However, some broadening of the TOF peaks is a small price to pay for essentially 100% transmission though the TOF tube with the guide wire potential on. Finally, by changing the ratio of the extraction to acceleration potentials, the relative positions of peaks corresponding to energetic charged fragments were varied with respect to those associated with thermal energies. This property of TOF spectrometers is very useful in interpreting the observed spectra (see also [8]).

The charged fragment times of flight T_r were extracted from the raw data as follows. Let T_0 be the time difference measured by the time-to-amplitude converter. T_0 consists of

$$T_0=T_r-T_p+T_d=k\times(\text{channel})+T'_{\text{MCA}}\ , \tag{1}$$

where T_p is the projectile time of flight from the interaction region to the $\pi/\sqrt{2}$ cylindrical electrostatic analyzer detector, and T_d is the sum of all electronic delays. On the right-hand side of Eq. (1), k represents the time per channel used to display the spectrum, and T'_{MCA} is any multichannel analyzer offset. Since T_d cannot be separated from T'_{MCA}, Eq. (1) can be written as

$$T_r=k\times(\text{channel})+T_{\text{MCA}}+T_p\ , \tag{2}$$

where T_{MCA} denotes all electronic delays.

Three different approaches were used to calibrate the TOF spectrometer. In the first, we used the recoil-ion spectrum produced in $2.3q$ keV Ar^{12+} on Ar collisions. Peaks corresponding to Ar^{q+} recoils ($1\le q\le4$) were identified, and from the dimensions of the instrument, the times T_r and T_p calculated. With the time-to-amplitude converter set to the 40 μsec scale, and using the calculated T_r and T_p values, we obtained, for k, 4.336×10^{-2} μsec/channel, and $T_{\text{MCA}}=3.23$ μsec. The calculated T_p

for Ar^{12+} was 1.11 μsec. For other argon projectiles of charge q extracted at 2.3 kV, $T_p^q = \sqrt{12/q}\ 1.11$. Equation (2) then becomes

$$T_r = [4.336\times10^{-2}\times(\text{channel}) + 3.23 + \sqrt{12/q}\ 1.11]\mu\text{sec} . \quad (3)$$

In the second approach, we measured the electronic delays directly. The $\pi/\sqrt{2}$ cylindrical electrostatic analyzer downstream from the interaction region was set to detect an Ar^{12+} beam extracted at 2.3 kV. The analyzer channeltron signal was split into two and fed through the same electronics used to generate both the start and stop time-to-amplitude converter pulses. The time difference between the signals was measured with a Tektronix model 2430A digital oscilloscope. The multichannel analyzer was then calibrated by delaying the time-to-amplitude converter stop signal with respect to the start signal. The variable delay between the start and stop signals was measured with the digital oscilloscope. The measured time delay precision was better than ±0.1 μsec, or about half the duration of the shortest chopping pulse used. On the 20-μsec time-to-amplitude scale, the error in the time calibration is, on the average, smaller than 0.5%. The calibration gave a value of $k = 4.299\times10^{-2}$ μsec/channel and a combined electronic and Ar^{12+} projectile time-of-flight delay of 4.78 μsec. The measured k is about 0.8% smaller than the calculated value, but the $T_{\text{MCA}} + T_p$ (for Ar^{12+}) is 0.44 μsec longer than the calculated value. The discrepancy between the two is most likely due to the calculated value of the recoil-ion time of flight, which assumes that all the electric fields in the spectrometer are well defined.

Under different experimental conditions, different time-to-amplitude converter (TAC) time scales had to be used, and/or inverted (TAC) spectra recorded. These required changes in the electronic delay, and it became impractical to measure the delays directly. Accordingly, to convert the raw TOF data to a time scale, we used the well-defined value of k, and the overall electronic delay was determined from the position of two known peaks in the spectrum. To this end we introduced, along with our target gases, small amounts of hydrogen. The positions of H_2^+ and the target molecular ion (e.g., CO^+, N_2^+) which bracket the TOF region of interest were then used to determine the overall electronic delay.

III. RESULTS

A. Ar^{q+} on N_2

We have measured the recoil-ion and molecular fragment time-of-flight spectra in Ar^{q+} on N_2 ($6 < q \leq 14$) collisions at 2.3q keV. The initial measurements were done using a medium-resolution, 50-cm-long TOF spectrometer. Since all of the spectra are qualitatively and quantitatively the same (Fig. 2), we present only representative results. The Ar^{8+} on N_2 spectrum is shown in Fig. 3. This spectrum was recorded at a 2 V extraction potential (electric field of 6.7 V/cm) and therefore higher-energy fragments were observed only when their velocities were parallel or nearly parallel to the electric field in the spectrometer interaction region. The most prominent peak at 33 μsec corresponds to the molecular ion N_2^+, while peaks with shorter flight times correspond to charged fragments of the target molecule. From the known geometry of the spectrometer and potentials applied to its various elements, we have calculated the positions of peaks corresponding to fragments of a given mass-to-charge ratio and initial kinetic energy, assuming that target ionization is essentially vertical. That is, the distance between the two nuclei of the target molecule remains unchanged during the collision, and hence the Coulomb explosion following the removal of two or more electrons from the target takes place at the equilibrium internuclear separation of the neutral molecule. Such an assumption is justified since the duration of the interaction between the projectile and target is about 1.7×10^{-15} sec (for a projectile kinetic energy of 23 keV and a 1×10^{-14} cm^2 total cross section), while the vibration period of the $^1\Sigma_g^+$ ground state of the N_2 molecule is about 1.4×10^{-14} sec [20].

The kinetic energies of the fragments produced in the breakup of the multiply charged molecular ion can therefore be calculated directly from the repulsive Coulomb potential energy of the fragments evaluated at the equilibrium separation of the molecule. We have calculated the time-of-flight peaks for all reasonable molecular ion fragments and charge distributions. In Figs. 3–7, the calculated flight times are shown as a series of vertical lines for each decomposition of the molecular ion into a fragment of a given charge (e.g., N^+) with the charge on the coun-

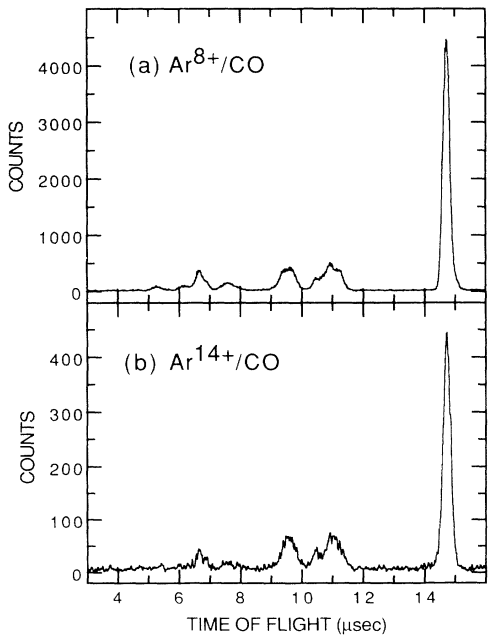

FIG. 2. Time-of-flight spectra of molecular ions and fragments produced in 2.3q keV collisions of (a) Ar^{8+} and CO, and (b) Ar^{14+} and CO. The sepctra were recorded with a 50-cm-long TOF spectrometer. They are virtually identical and representative of the general observation that, for N_2 and CO, the sepctra do not depend on the argon-projectile charge state.

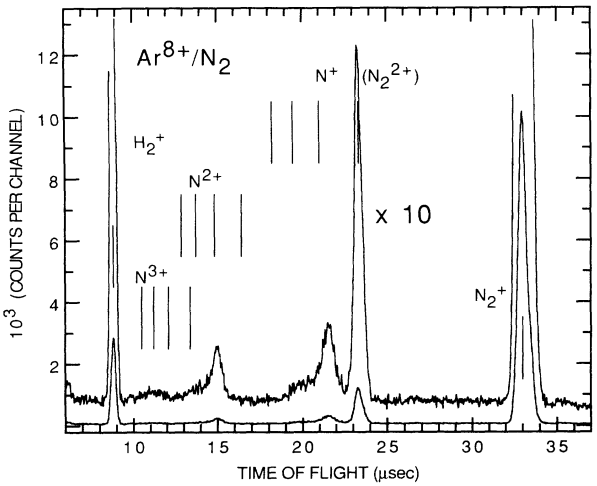

FIG. 3. Time-of-flight spectrum of molecular ions and fragments produced in $2.3q$ keV collisions of Ar^{8+} on N_2. The spectrum was recorded with a 50-cm-long TOF spectrometer. The vertical lines represnt flight times for a given breakup of the molecular ion into fragments of the indicated charge, and counterfragments of charge 0 (rightmost line) to 3+ (leftmost line), respectively. A small amount of H_2 was introduced along with the target gas for TOF calibration. The vertical scale refers to the $\times 10$ spectrum.

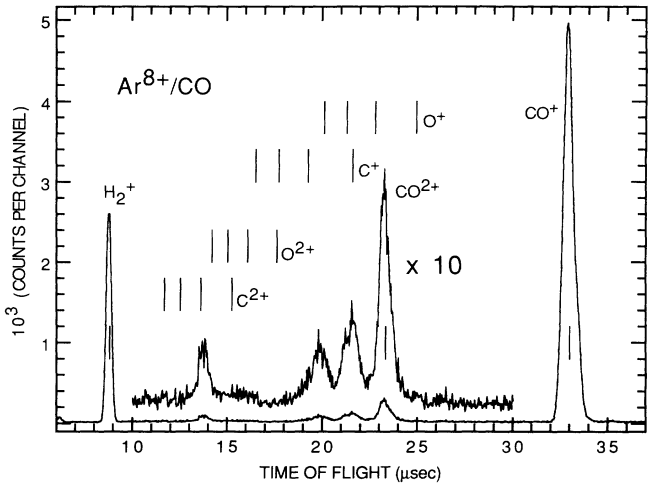

FIG. 5. Time-of-flight spectrum of molecular ions and fragments produced in $2.3q$ keV collisions of Ar^{8+} on CO. The spectrum was recorded with a 50-cm-long TOF spectrometer. The vertical scale refers to the $\times 10$ spectrum. The most prominent feature in the $\times 10$ spectrum is the stable or long-lived metastable doubly charged molecular ion CO^{2+}.

terfragment varied from 0 to 3+. The rightmost line in each series corresponds to a breakup into a fragment with the indicated charge plus a neutral counterfragment. The second from the right line indicates a breakup into a fragment with charge +1 (e.g., N^+), and so on.

Hence, in Fig. 3, the second rightmost peak around 23.5 μsec corresponds to a breakup of N_2^+ into a thermal energy N^+ and a neutral atom N^0. However, the molecular ion N_2^{2+} can contribute significantly to this peak because its mass-to-charge ratio coincides with that of a thermal energy N^+ ion. The smaller peak at 21.5 μsec corresponds to N^+ ejected from N_2^{2+}. The slight tail of this peak which extends towards shorter flight times is due to N^+ ejected from N_2^{3+}. The calculated positions are marked by vertical lines, and the agreement with observed flight times is excellent. As for the N^{2+} fragments, the peak at 15 μsec is due to the breakup of N_2^{3+} into N^{2+} and N^+. The absence of a thermal energy N^{2+} peak clearly shows that two-electron capture from the molecule followed by its breakup into N^{2+} and N^0 is highly unlikely. The poorly resolved structure above 10 μsec corresponds to breakups in which one

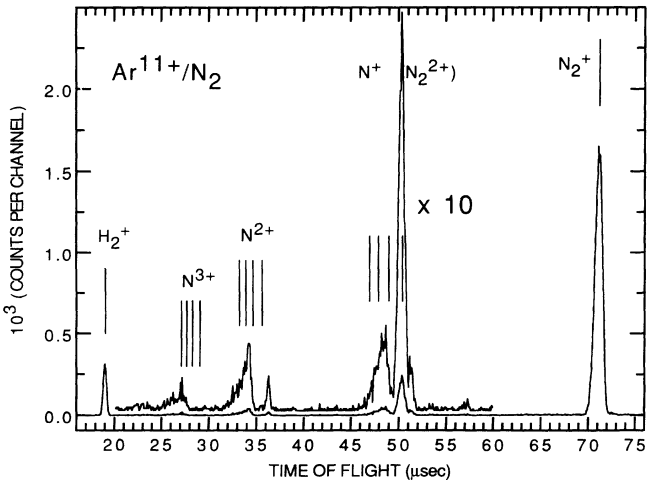

FIG. 4. Time-of-flight spectrum of moelcular ions and fragments produced in $2.3q$ keV collisions of Ar^{11+} on N_2. The spectrum was recorded with a 2.5-m-long TOF spectrometer at 10 V extraction potential. The vertical scale refers to the $\times 10$ spectrum.

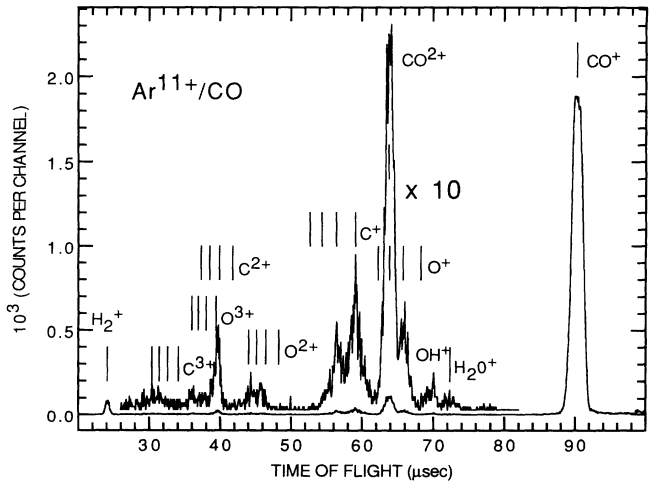

FIG. 6. Time-of-flight spectrum of moelcular ions and fragments produced in $2.3q$ keV collisions of Ar^{11+} on CO. The spectrum was recorded with a 2.5-m-long TOF spectometer at 6 V extraction potential. The vertical scale refers to the $\times 10$ spectrum.

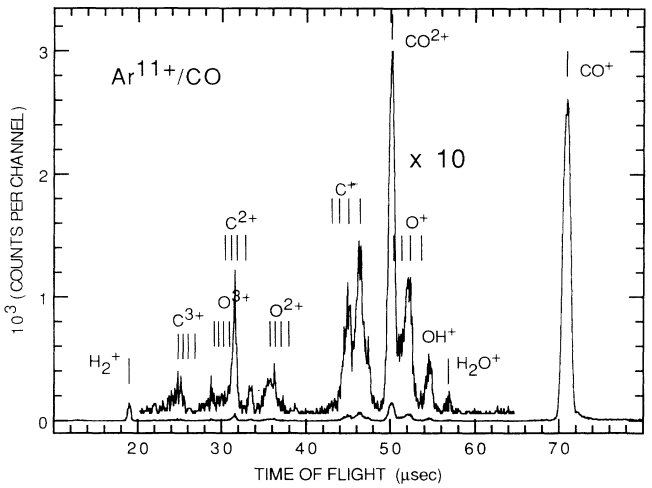

FIG. 7. Time-of-flight spectrum of moelcular ions and fragments produced in $2.3q$ keV collisions of Ar^{11+} on CO. The spectrum was recorded with a 2.5-m-long TOF spectometer at 10 V extraction potential. The vertical scale refers to the $\times 10$ spectrum.

would expect N^{3+} fragments. The thermal kinetic-energy N^{3+} peak is masked by peaks which belong to N^{2+} fragments with higher kinetic energies, namely those associated with counterfragments of charge 2+ and 3+. Such fragments are produced following the capture of four or five electrons from N_2. From this singles spectrum it is not possible to determine the relative contribution of thermal energy N^{3+} and energetic N^{2+} ions.

Similar spectra were recorded with out 2.5-m-long instrument. The TOF spectrum for Ar^{11+} on N_2 is shown in Fig. 4. In this case, the extraction potential was 10 V, (corresponding to the same electric field of 6.7 V/cm as in the short instrument). Again, the N_2^+ molecular peak at 71 μsec is the most prominent feature. As in Fig. 3, N^+ fragments are observed with kinetic energies that correspond to counterfragments of charge 1+ and 2+. The thermal energy N^+ peak is obscured by the N_2^{2+} peak. The N^{2+} fragments peak at flight times indicating that they originate from N_2^{3+} and N_2^{4+}. The sharp peak around 36 μsec is due to a N^{2+} fragment associated with N^+, which is slowed down, and then reflected back into the TOF spectrometer. Such ions should arrive about 1.24 μsec later than those directed into the spectrometer, or parallel to the electric field in the ionization region. The calculated time of flight agrees quite well with the observed 36 μsec. A similar reflection occurs at the tail of the thermal energy peak corresponding to $m/q=14$, which extends toward longer flight times. The calculated flight time for a N^+ fragment ejected from N_2^{2+} in the direction opposite the electric field in the ionization region is 50.8 μsec, again in fair agreement with an observed small peak on the right flank of the N^+, N_2^{2+} peak.

The structure around 27 μsec is associated with fragments of charge 3+ ejected from the molecular ions N_2^{6+} and N_2^{5+}. From the figure, it is clear that there are no N^{3+} thermal energy fragments.

The measured TOF spectra indicate that in collisions of highly-charged-argon ions with molecular nitrogen, the molecule can lose up to six electrons. Following charge redistribution to both nuclei, the highly charged molecular ion breaks up into fragments with equal or similar charges. In the present experiment, one-electron capture from the molecule which leads to dissociation cannot be separated from two-electron capture, which produces the relatively stable states of the N_2^{2+} ion [21]. Two-electron capture can also result in the formation of repulsive states of N_2^{2+}, which then break up into two N^+ ions that recoil from one another, each fragment with 6.61 eV kinetic energy. Three-electron capture is followed by break up into N^+ and N^{2+}, and there is no evidence of charge partitioning into N^{3+} and N^0. When four electrons are removed from the target, the fragmentation leads preferentially to two N^{2+} ions. Break up into N^+ and N^{3+} occurs with a much lower probability. There was no indication of thermal energy N^{4+} ions, even though the instrument has essentially 100% collection efficiency for very-low-energy ions. The capture of five and six electrons from the target results mainly in the fragments N^{3+}, N^{2+}, and N^{3+} respectively. That is, $N_2^{5+} \rightarrow N^{2+} + N^{3+}$, and $N_2^{6+} \rightarrow N^{3+} + N^{3+}$.

The relative contributions of N_2^{2+} and thermal kinetic-energy N^+ ions to the peak corresponding to mass-to-charge ratio $m/q=14$ cannot be ascertained, unfortunately. One would have to use a known $^{15}N^{14}N$ isotopic mixture as a target, but even in this case it would be difficult to unravel the spectra with our instrument. To obtain an estimate of the relative number of doubly charged molecular ions created during the collision, we used CO as a target. The CO molecule is isoelectronic with N_2 and has the same molecular weight.

B. Ar^{q+} on CO

As in the case of the molecular nitrogen target, we used a 50-cm-long version of our TOF spectrometer in the preliminary studies. Figure 5 shows the time-of-flight spectrum of molecular fragments produced in collisions of $2.3q$ keV Ar^{8+} with CO at 2 V extraction potential. In contrast to the molecular nitrogen target, the peak at 23.3 μsec corresponds to CO^{2+} alone, with no accompanying interference from any other species. The entire spectrum is more complicated because the multiply charged CO^{Q+} molecular ion breaks up into fragments which can differ both in charge and mass. The fragments share the Coulomb potential energy of repulsion according to conservation of energy and momentum.

The most prominent peak at 33 μsec is associated with one-electron capture from CO. Following one-electron capture from CO, the molecule ends up in one of the stable electronic states of CO^+, most probably the $X\,^2\Sigma^+$ ground state and perhaps the low-lying $A\,^2\Pi_i$ and $B\,^2\Sigma^+$ excited states [22]. However, breakup into C^+ and O^0 can also occur, as can be inferred from the peak at 21.6 μsec. On the other hand, the complementary process which leads to $O^+ + C^0$ does not show up in Fig. 5. This behavior can be understood in terms of the electronic states available to the fragments. The lowest-energy asymptotic breakup channels correspond to

$C^+(^2P)+O(^3P)$ and to $C^+(^2P)+O(^1D)$, while the first channel leading to $C(^3P)+O^+(^4S)$ lies about 2.4 eV above the $C^+(^2P)+O(^3P)$ ground state [22].

Two-electron capture, followed by a Coulomb explosion which produces the fragments C^+ and O^+ shows up as the peak at 19.3 μsec, C^+ repelled by O^+, and a smaller peak at 22.8 μsec, O^+ repelled by C^+. The latter appears as a shorter flight time tail on the CO^{2+} peak. Three-electron capture from CO is followed by breakup into $C^{2+}+O^+$. There is little evidence in Fig. 5 for the breakup resulting in C^++O^{2+}. No thermal energy fragments with charge 3+ were observed, which seems to confirm the general observation of equal or almost equal charge distribution between the fragments following two or more electron capture by the molecule.

Figure 6 shows the TOF spectrum of fragments produced in $2.3q$ keV Ar^{11+} on CO collisions. The extraction potential was 6 V (electric field of 4 V/cm). The spectrum shows features similar to those observed in Fig. 5 with the shorter TOF spectrometer, but at much better resolution. Although in this case the CO^{2+} peak at 63.8 μsec coincides with the time of flight of a O^+ fragment repelled by C^{2+}, the contribution of the latter process can be estimated to be about 10–20% of the total intensity from the other spectra (e.g., Fig. 7) where the peaks are distinguishable. Four-electron capture, which is not seen in Fig. 5, brings about an equal sharing of charge. The corresponding fragments show up as weak peaks at 39 μsec, C^{2+} repelled by O^{2+}, and at 45.5 μsec, O^{2+} repelled by C^{2+}. We observed no breakup into asymmetrically charged fragments, nor did we see any thermal fragments with charge 4+. Five-electron capture leads predominantly to $C^{3+}+O^{2+}$ breakup, as can be seen from the peaks at 44 μsec which correspond to O^{2+} repelled by C^{3+}, and at about 31.3 μsec, C^{3+} repelled by O^{2+}. The complementary breakup which would lead to $C^{2+}+O^{3+}$ was not observed, and it is very likely that the reason for preferential decomposition of CO^{5+} into $C^{3+}+O^{2+}$ is similar to that observed in the beakup of CO^+ and CO^{3+}. Finally, if the target loses six electrons, the charge is divided equally between the fragments C^{3+} and O^{3+}, which are by far the most important products.

These conclusions were also confirmed in the spectra recorded with the 2.5-m-long TOF spectrometer at an even higher extraction voltage of 10 V, as shown in Fig. 7. In this case, there could be a contribution to the CO^{2+} peak from O^+ produced by the decomposition of CO^{4+}, but since the counterfragment C^{3+} does not appear at all in the spectrum, the CO^{2+} peak has no interfering ions. Moreover, such fragmentation is very unlikely as can also be seen from Figs. 5 and 6. As observed in Fig. 4, the 10-V extraction potential can cause reflection of low-energy fragments emitted in the direction opposite to the extracting field. Such a reflection appears at 33.5 μsec. in Fig. 7, and could easily be mistaken for thermal C^{2+}. However, comparison of spectra recorded at different extraction voltages excludes this possibility. Calculations of the flight time of C^{2+} recoiling from O^+ in the direction opposite to the extracting field shows that such reflected ions should arrive at 33.25 μsec. Similar reflection of C^+ ions recoiling from O^+ causes broadening of the thermal C^+ peak.

IV. CONCLUSIONS

The formation and breakup of molecular ions created in $2.3q$ keV collision of Ar^{q+} with N_2 and CO are independent of the incident projectile charge q for $8 \le q \le 14$. The singly charged ions N_2^+ and CO^+ seem to dominate the TOF spectra. However, these ions have thermal energies, and because of the unknown collection efficiency of the TOF spectrometer for the more energetic ions, it is not possible to determine the relative intensities of the various fragments. This is in contrast with the measurements of the recoil-ion charge-state distributions in Ar^{q+} on Ar collisions [13], where the recoils have thermal energies and the detection efficiency for all such ions by the TOF spectrometer is close to 100%. The stable or long-lived metastable doubly charged molecular ions N_2^{2+} and CO^{2+} formed in two-electron capture from the target are created in appreciable quantities. This would suggest that intense, low-energy, highly charged-ion beams from an electron cyclotron resonance (ECR) source could be used to produce these interesting species.

The peaks in the TOF spectrum corresponding to fragments of a given mass-to-charge ratio and kinetic energy were identified by assuming vertical target ionization. That is, the kinetic energy of the fragments was calculated from the Coulomb potential energy evaluated at the equilibrium internuclear separation of the neutral molecule for different redistributions of charge on the two atoms following the capture of two or more electrons from the molecule. The excellent agreement between the calculated and observed TOF peak positions indicates that the distance between the two nuclei of the target molecule remains unchanged during the collision and subsequent Coulomb explosion of the molecular ion. All spectra show that up to six electrons can be removed from the target molecule in collision with highly charged Ar ions at $2.3q$ keV projectile energy. The subsequent breakup of the molecular ion CO^{Q+} leads preferentially to channels with equal fragment charges (Q even), or to channels $C^{[(Q+1)/2]+}+O^{[(Q-1)/2]+}$ (Q odd).

ACKNOWLEDGMENTS

We would like to thank J. J. Perotti for constructing most of the apparatus used in the experiment and for his invaluable advice in matters pertaining to apparatus design. This work was supported in part by the U.S. Department of Energy, Office of Basic Energy Sciences, Division of Chemical Sciences, under Grant No. DE-FG02-86ER13519.

[1] R. K. Janev and H. Winter, Phys. Rep. **117**, 265 (1985).
[2] M. Kimura and N. F. Lane, Adv. At. Mol. Opt. Phys. **26**, 79 (1990).
[3] W. Fritsch and C. D. Lin, Phys. Rep. **202**, 1 (1991).
[4] K. Wohrer, G. Sampoll, R. L. Watson, M. Chabot, O. Heber, and V. Horvat, Phys. Rev. A **46**, 3929 (1992).
[5] G. Sampoll, O. Herber, R. J. Maurer, P. A. Scott, and R. L. Watson, Nucl. Instrum. Methods Phys. Res. B **40-41**, 308 (1989).
[6] I. Ben-Itzhak, S. G. Ginther, and K. D. Carnes, Phys. Rev. A **47**, 2827 (1993).
[7] D. Mathur, E. Krishnakumar, F. A. Rajgara, U. T. Raheja, and V. Krishnamurthi, J. Phys. B **25**, 2997 (1992).
[8] S. L. Varghese, C. L. Cocke, S. Cheng, E. Y. Kamber, and V. Frohne, Nucl. Instrum. Methods Phys. Res. B **40-41**, 266 (1989).
[9] K. Soejima, C. J. Latimer, K. Okuno, N. Kobayashi, and Y. Kaneko, J. Phys. B **25**, 3009 (1992).
[10] T. K. McLaughlin, R. W. McCullough, and H. B. Gilbody, J. Phys. B **25**, 1257 (1992).
[11] J. Vancura and V. O. Kostroun, in *Proceedings of the Ninth European Conference on Dynamics of Molecular Collisions,* edited by Z. Herman (Czech Acad. of Sciences, Prague, 1992), p. 203.
[12] H. Lebius and B. A. Huber, in *Proceedings of the VIth International Conference on the Physics of Highly Charged Ions,* edited by P. Richard, M. Stockli, C. L. Cocke, and C. D. Lin, AIP Conf. Proc. No. 274 (AIP, New York, 1993), p. 218.
[13] J. Vancura and V. O. Kostroun, in *Proceedings of the VIth International Conference on the Physics of Highly Charged Ions* (Ref. [12]), p. 113
[14] R. I. Hall, A. McConkey, L. Avaldi, M. A. McDonald, and G. C. King, J. Phys. B **25**, 411 (1992).
[15] N. Levasseur, Ph. Millie, A. Archirel, and B. Levy, Chem. Phys. **153**, 387 (1991).
[16] V. O. Kostroun, in *Proceedings of the International Symposium on Electron Beam Ion Sources and their Applications,* edited by A. Herschcovitch, AIP Conf. Proc. No. 188 (AIP, New York, 1989), p. 65.
[17] W. C. Wiley and I. H. McLaren, Rev. Sci. Instrum. **26**, 1150 (1955).
[18] J. Abbe, S. Amiel, and R. D. McFarlane, Nucl. Instrum. Methods **102**, 73 (1972).
[19] Electrostatic lens analysis and design program SIMION, PC/PS2 version 4.0. Idaho National Engineering Laboratory, EG&G Idaho Inc. Idaho Falls, ID 83415.
[20] G. Herzberg, *Spectra of Diatomic Molecules* (Van Nostrand-Reinhold, Princeton, 1950).
[21] N. Levasser, Ph. Mille, P. Archirel, and B. Levy, Chem. Phys. **153**, 387 (1991), and references therein.
[22] J. B. Hasted, *Physics of Atomic Collisions,* 2nd ed. (American Elsevier, New York, 1972).